Projection-Reconstruction Spectroscopic Imaging for B_0 Field Plotting and Shimming without Pulsed Gradients

Carl D. Gregory

Biomedical Magnetic Resonance Laboratory, University of Illinois at Urbana–Champaign, 1307 West Park Street, Urbana, Illinois 61801

Shimming is important. Noniterative methods are desirable. Such methods exist for shimming a spectrometer with pulsed field gradients, generally based on field maps made by spin-warp Fourier imaging. For spectrometers with no pulsed gradients (or for cases where T_2 is too short to permit echo imaging), an alternative method is presented: projection-reconstruction spectroscopic imaging, which can be accomplished using only the shim coils of a conventional spectrometer. Images so acquired can be used to map the field, even in the presence of multiple spectral components. Noniterative optimization of the axial shims of a GN-300 spectrometer is demonstrated using 1D + 1D spectroscopic images. Prospects for extending the technique to include the radial shims using 3D + 1D spectroscopic images are discussed. © 1997 Academic Press

Key Words: **shimming; field mapping; projection reconstruction; spectroscopic imaging; B_0 homogeneity.**

INTRODUCTION

Shimming an NMR spectrometer has traditionally been an empirical art (*1–3*). Apprentice spectroscopists practice many hours, memorizing protocols for iterative shimming and empirical rules for evaluating lineshapes, on the road to competence in shimming. Early automatic shimming systems, many still in use today, simply automated these procedures, using numerical optimization techniques such as the ''simplex'' method (*4*) to optimize a single response such as lock level, FID area, or peak height. Such iterative searches, or empirical rules (e.g., separation of shims into ''spinning'' and ''nonspinning'' components), have proven reasonably successful in shimming homogeneous liquid samples. This is partly because once the radial shim terms have been coarsely optimized, it is seldom necessary to make large changes in their settings. Nevertheless, certain situations are still very difficult, including installation of a new probe, large-diameter samples, and inhomogeneous samples such as tissue specimens. In all three of these cases, optimization of the nonaxial shim terms, with their extensive interactions, constitutes the major difficulty. The use of a single numerical response (such as lock level or linewidth) or a limited number of responses (such as linewidths at 50,

0.55%, etc.) makes it difficult to unambiguously and simultaneously optimize dozens of shim currents. Susceptibility to noise or instrumental instability, excessive time requirements, and the eternal problem of local optima also limit the utility of the iterative methods when all shims must be optimized.

Recently, the concept of quantitative field mapping (*5, 17*), originally applied to large magnets for medical imaging, has been brought to smaller spectroscopy magnets. Originally, this was done with mechanical positioning systems and small probes, but more recently, adaptation of imaging techniques using pulsed field gradients (PFG) has permitted *in situ* measurement of the actual field in a sample of interest in a reasonable time period (*6–15*). Rather than using a single response to characterize the field, mapping methods use many simultaneous responses to simultaneously (and hopefully independently) optimize all of the shim currents. Aside from the practical value of directly shimming the magnet, the field maps themselves may be interesting for the insight they give into sample- or probe-dependent field distortions, as well as for pedagogical purposes.

In situ field mapping techniques offer the greatest promise for high-resolution spectroscopy, since they take into account the effects on the field of the probe, sample tube, and sample itself. These methods fall into three broad categories: (I) nonimaging methods; (II) phase-imaging methods; and (III) frequency-imaging (or spectroscopic imaging, SI) methods.

Nonimaging methods include the direct, sequential, measurement of the spectrum at selected points using VOSY (*7, 16*) which is a straightforward extension of well-established sequential mapping procedures using mechanical positioning of a small field probe. A variation (*12*) obtains multiple points simultaneously along principal axes and diagonals of a cube. These methods will not be further considered, as they generally require PFG for signal localization.

Phase imaging can be considered a subset of frequency imaging. If it is known that only one spectral component is present, and the range of frequency values for that component is limited, it is sufficient to obtain two complex images

with slightly different time delays. The phase difference between the images can then be interpreted as a frequency (or field) variation. A number of authors have developed these techniques using phase-encoded (''spin-warp'') imaging methods with PFG (*6, 8, 10, 11, 13*). An interesting variant, not necessarily requiring PFG, uses the ''constant-time method'' (*15*) with static gradients. A spatial–spectral excitation method has also been used to overcome phase ambiguities resulting from multiple components (*10*).

If, as is often the case, the criteria for phase mapping are not satisfied (e.g., multiple spectral components are present, or the phase-wrap problem is intractable due to gaps in the object), then more samples will be required to define the frequencies—a full-fledged spectroscopic image is required. Frequency mapping techniques have also been demonstrated (*9, 14, 17*), again based on phase encoding with PFG.

The use of PFG excludes most of these published techniques from use on older spectrometers. (Although some older instruments do have a ''homospoil'' control which allows pulses on the Z shim coil, these permit mapping the Z axis only (*34*).) Pulse methods may also be difficult to use with samples which have a very short T_2. However, there is an alternative—projection-reconstruction spectroscopic imaging (PRSI) (*18–20*). PRSI, originally demonstrated for NMR, has been more widely developed for EPR due to the technical requirements of the latter field (*21–27*).

Like its cousin, pulsed-gradient, phase-encoded, Fourier spectroscopic imaging (FSI), PRSI generates an $(n + 1)$-dimensional data set: n spatial dimensions, and one spectral (frequency, or in this case, field) dimension. Unlike its cousin, PRSI requires no PFG. FIDs or echoes are acquired in the presence of static field gradients, which for our purposes can be generated by ordinary shim coils. Separation of the frequency and spatial information is obtained by varying the gradient strength G, using a pseudo-angle θ (*19*). Note that a change in the spectral width, $\Delta\omega$, for each projection is also required:

$$\theta = \arctan\left(\frac{\gamma GD}{\Omega}\right) \quad \text{and} \quad \Delta\omega = \frac{\Omega}{\cos\theta} \qquad [1]$$

(D, spatial field of view; Ω, spectral field of view). $\theta = 0°$ thus corresponds to a pure spectral projection, while $\theta = \pm 90°$ would be a pure spatial projection (impossible because it requires an infinite gradient).

In addition to the pseudo-angle (between the spectroscopic dimension and the spatial dimensions) which depends on the *strength* of the gradient, the *spatial direction* of the gradient vector can also be varied in the usual way, using X, Y, and Z^1 shims. This variation is generally described by two real spatial angles (e.g., polar and equatorial). Thus, while the present report deals only with gradients along one axis, multiple spatial dimensions can be handled by a

straightforward extension, as has been shown by others (*19, 26–29*). A four-dimensional SI experiment then would have the following acquisition variables: FID points; gradient strength; polar gradient angle α (from z axis); equatorial gradient angle β (in x–y plane). These reconstruct to one spectral and three spatial dimensions.

In this report, the application of PRSI to field mapping and shimming is illustrated using field maps with one spatial dimension (1D + 1D PRSI) to adjust the axial shims of a conventional NMR spectrometer. The feasibility of carrying out a complete shim using full 3D + 1D PRSI maps (*26–29*) is under investigation.

EXPERIMENTAL

All experiments were conducted on a GN-300 WB spectrometer (GE-NMR, Fremont, CA), equipped with a Libra system (Tecmag, Houston, TX) replacing the original Nicolet 1280 computer, but otherwise unmodified. The ^{1}H decoupler coil of a 20-mm broadband probe (Nalorac, Martinez, CA) was used for all measurements. The measured gradient strength of the Z^1 coarse shim system was 105 Hz/mm at the maximum digital-to-analog converter (DAC) values (± 2047). Settling times of this shim current are difficult to measure, but are probably on the order of a second.

Samples consisting of distilled water or aqueous solutions were used for the experiments. A 5-mm NMR tube (Wilmad WG-5mm-Thrift) was filled to a depth of 60–90 mm with sample, and mounted vertically in the probe using the GE depth gauge to estimate position. Use of a small sample tube avoids radiation damping problems and reduces complications due to off-axis field contributions from the axial shim coils. (No particular effort was made to optimize the radial ''nonspinning'' shims.) The samples were stationary, and the field/frequency lock was turned off since the solvent was not deuterated.

Mapping data were acquired using a simple one-pulse sequence with FID acquisition. A small flip angle (5°) was used to obtain uniform excitation across the widest projection bandwidth used. With a $\pi/2$ pulse measured at 90 μs ($B_1 = 2.8$ kHz), and a maximum spectral width of ± 4075 Hz, a 5-μs RF pulse provides excitation across the entire projection with better than 99% uniformity. A 1-s delay was included between setting the shim current and the beginning of the pulse sequence. Water-suppressed spectra of aqueous solutions were obtained using the 1–1 spin-echo sequence (*32*), with delays chosen to optimize signal at 1 kHz offset, 2 ms echo time, 7 s repetition time, and 16 averages.

The PRSI acquisition procedure is similar to that reported in (*19*). A complete set of n projections was acquired at equally spaced pseudo-angles over the range $-\pi/2 + \pi/2n \leq \theta \leq \pi/2 - \pi/2n$, thus avoiding the physically impossible $\theta = \pi/2$. PRSI requires that both the gradient and the spectral width be changed together, according to Eq. [1]. The preac-

quisition delay and the audio filters were also adjusted automatically for each projection to eliminate any first-order phase corrections (*30*). An NMRScript automation routine was written to facilitate this procedure. After querying the operator for selection of the field of view (FOV) (typically 5–10 cm along the Z axis and 100–400 Hz in the spectral dimension) and number of projections (typically 8 to 64), the routine calculates the correct spectral width, preacquisition delay, and Z shim setting for each projection according to Eq. [1], taking into account the starting value of the Z shim. The spectrometer is automatically set up for each projection, and the acquired data are stored into a 2D data file for subsequent processing. The experiments reported here used FOV 10 cm × 200 Hz, 64 values of θ from 88.6° to −88.6°, and spectral widths $\Delta\omega$ from 200 to 8150 Hz.

Filtered projections were generated by Fourier transforming the FIDs after multiplication by an appropriate weighting function (*27*). A combination of a high-k-value rolloff and a linear ramp function ($|k|$) are generally used for two-dimensional reconstructions. Instead of the Hamming or Shepp–Logan filters commonly used for ordinary imaging, a Lorentzian spectroscopic line broadening (1–5 Hz) was used for the high-frequency rolloff, in part because of the convenience of application in the spectrometer software. The linear ramp was implemented using the spectrometer's "trapezoidal multiplication" function. Zero-order phase correction was applied as required after the transform.

Various reconstruction methods are possible, such as back-projection, or interpolation followed by Fourier transform. Back-projection was chosen in this case as a matter of convenience and availability of software. The real part of the phased, filtered projections was used to reconstruct spectroscopic images via back-projection, using *viewit* (*33*), an all-purpose software package. In some cases, additional projections were interpolated in the sinogram between the real ones using a linear interpolation scheme (i.e., angular interpolation only). Peak picking (selection of the maximum intensity value, with or without a preceding sinc interpolation) in the spectral dimension reduced the images to one-dimensional field maps, which were exported from *viewit* as text files. Least-squares fitting for shim correction and 1D plotting were done using Excel spreadsheets (Version 5.0, Microsoft, Redmond, WA).

Field maps for each of the five individual axial shim coils (labeled Z^1, Z^2, Z^3, Z^4, and Z^5) were obtained by mapping the field twice with different settings of the respective shim DAC (range ±2047). For Z^1, Z^2, and Z^3, the fine DAC was varied, while the coarse DAC was held constant (except for Z^1 where the coarse DAC was used to generate the projections). Since a single reference map was used for all five coils, a total of six maps was required.

Shim corrections were estimated from a field measurement by conventional procedures (*8–10, 13, 14*). The unknown field $B(z)$, to be corrected, is fitted directly to a sum of fields of the individual coils (rather than using an intermediate analysis in terms of spherical harmonics). The coefficients c_j for j coils are determined by ordinary linear least-squares fitting,

$$B(\mathbf{z}) = c_0 + \sum_j c_j \cdot \beta(\mathbf{z})_j + \epsilon(\mathbf{z}), \qquad [2]$$

where the c_j are chosen to minimize the sum of squares of the residuals $\epsilon(z)$. Since the individual coil fields $\beta(z)$ were determined at known DAC offsets Δd, the coefficients c_j can be simply interpreted as

$$c_j = \delta d_j/\Delta d_j \quad \text{or} \quad \delta d_j = c_j \cdot \Delta d_j, \qquad [3]$$

where $-\delta d_j$ is the DAC correction to be applied to the jth coil to homogenize the field. As noted by others (*9, 10*), the constant term c_0 is required to compensate for any field offsets, but it is either ignored when adjusting the shim currents or compensated by changing the spectrometer frequency slightly.

RESULTS

Field Maps

To illustrate the PRSI principle, a raw data set is shown in Fig. 1 as a stacked plot of projections (a "sinogram"). This data set was acquired with the Z^4 shim deliberately misset. The characteristic shapes of the projections (*2, 3*) are evident in the stacked plot. The same data are displayed after reconstruction as a gray-scale spectroscopic image in Fig. 2e, and as a field map (plot of frequency vs position) in Fig. 4d. The B_1 profile of this decoupler coil, obtained by summing over the spectral direction, is shown in Fig. 3. Note that this is the purely spatial profile of the coil, which would require an infinite gradient for direct observation.

A complete set of spectroscopic images, of each of the shim coils, is shown in Fig. 2, together with the "reference" image (with the axial shims all optimized using the spectrometer's built-in simplex autoshim routine). Each of these images can be integrated over frequency to give the same B_1 profile as shown in Fig. 3.

The peak positions, extracted from the images of Fig. 2, and corrected by subtraction from the reference map, are plotted in Fig. 4 as graphs of field strength vs axial position for each of the shim coils. The plots are limited to the central region of highest probe sensitivity (±14.5 mm, the region containing 93% of the total signal, and over which response for this flip angle is more than 25% of the peak value—see discussion below). Of course, one could use other limiting criteria, thus carrying out a "localized shim," if desired (*8*).
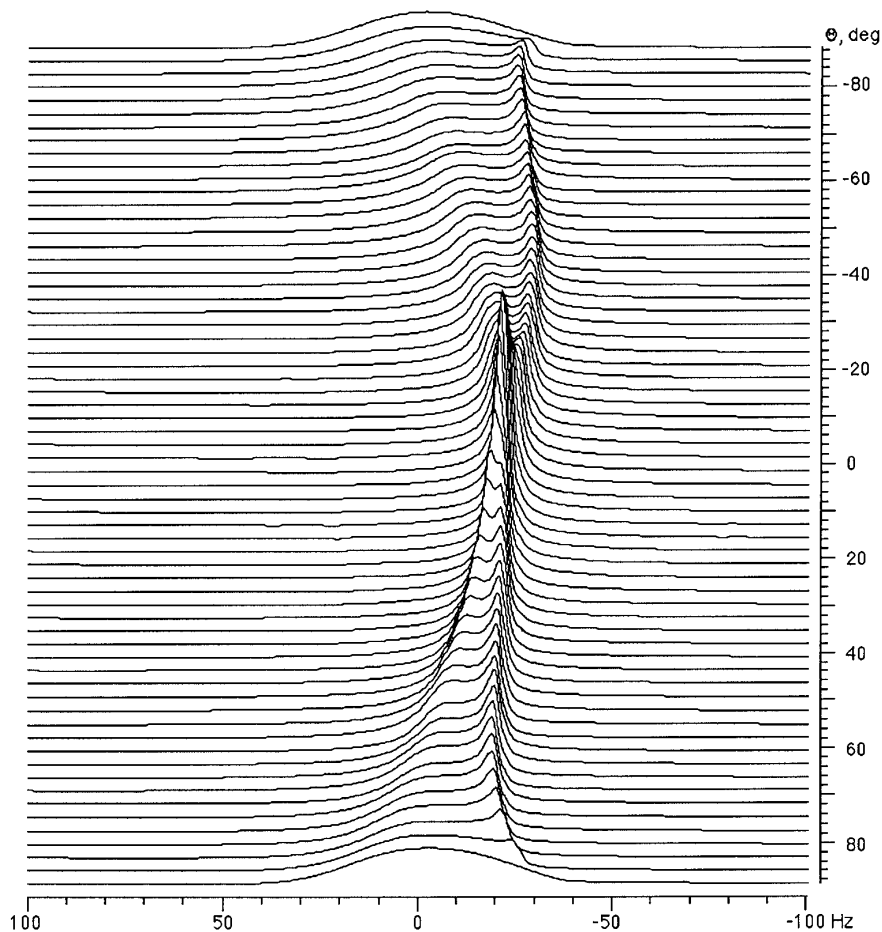
FIG. 1. Projection sinogram of the Z^4 shim coil: stacked plot of projections at 64 pseudo-angles from 87° to −87°. The ω axis is labeled to correspond to the spectral width for $\theta = 0$ (2 Hz line broadening).

Estimation of Known Perturbations

Once the complete set of shim coil field maps was obtained, an attempt was made to numerically shim the magnet starting from ''unknown'' situations. First, a series of known perturbations was applied to the field.

Three, four, or five of the axial shims (Z^1–Z^5) were deliberately misset by small amounts (50 DAC units each). The field was mapped again using the same procedure each time. A linear combination of shim fields was determined by linear least squares, using the previously obtained basis set, to fit each of the perturbed fields. The resulting coefficients, interpreted as shim current DAC values according to Eq. [3], were then entered into the spectrometer control software. The resulting lineshapes were essentially indistinguishable from the reference lineshape (FWHM 1.3 ± 0.1 Hz). The fitted or ''predicted'' DAC values are shown in Table 1, along with the standard errors of estimate. The matrix of correlation coefficients between the individual coil maps is shown in Table 2.

Shimming ''Unknowns''

To simulate a more realistic situation, the sample was moved 10 mm up in the sample holder. This represents the sort of situation one might have to deal with, for example, when changing samples. The difference in susceptibility between the sample and the air beyond the ends of the sample causes a field distortion which depends on the sample position and the depth of liquid in the sample tube. A new map was generated, shim corrections were computed and applied, and the new spectrum and image were recorded. The spectroscopic images of the sample after the move, and after the correction, are shown in Fig. 5, while spectra showing the overall lineshape before (FWHM = 4 Hz) and after (FWHM = 1.3 Hz) are in Fig. 6.

Finally, the sample was replaced with a sample containing 5 mM lactic acid in a physiological buffer. The field was mapped on the new sample, the shim corrections were applied, and a water-suppressed spectrum was obtained. Water suppression is a particularly severe test of shimming, since
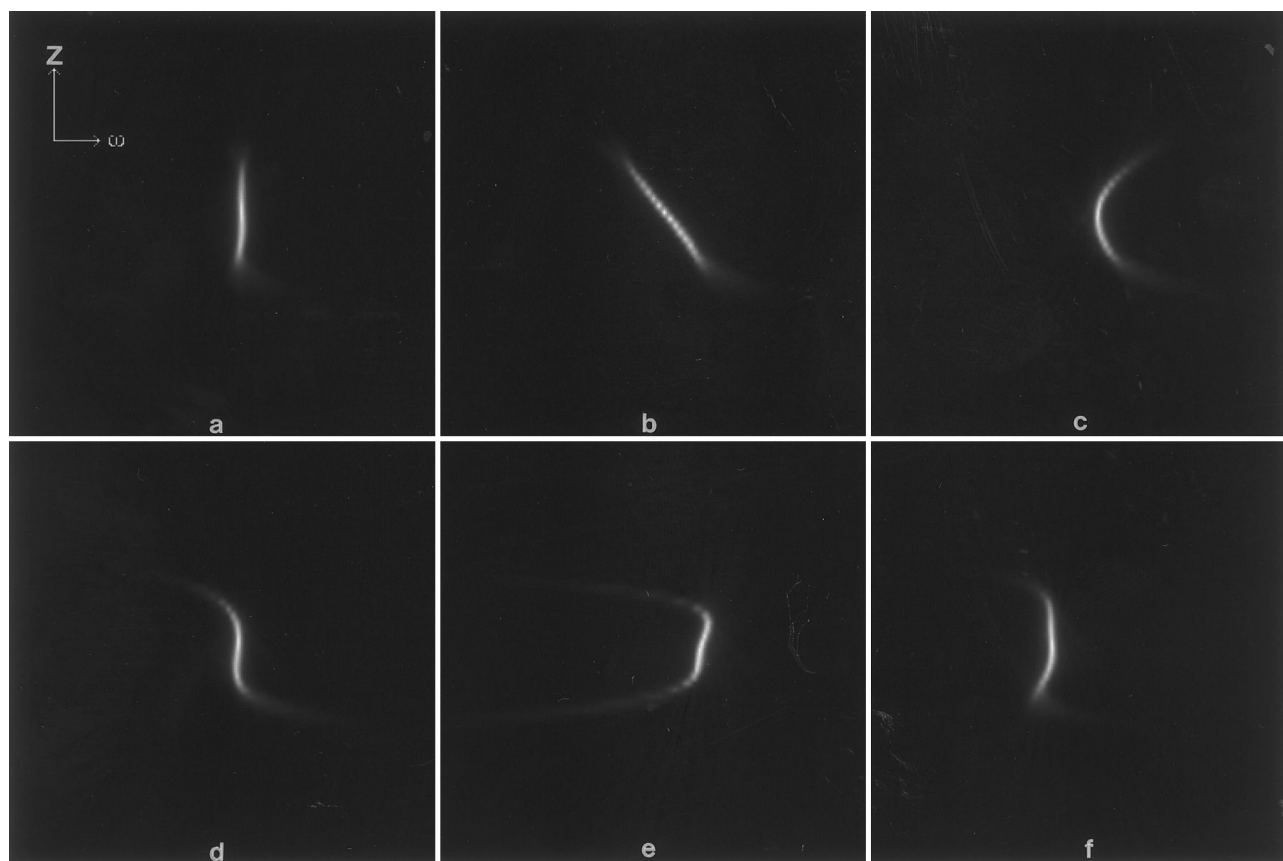
FIG. 2. Spectroscopic images of a 5-mm tube of water subjected to each of the axial shim coil fields. Field of view same as in Fig. 1 (200 Hz × 100 mm). Vertical axis is position, and horizontal axis is field (frequency). (a) Reference image, all DACs at ''best'' value; (b) Z^1 fine DAC − 400; (c) Z^2 fine DAC − 800; (d) Z^3 fine DAC − 700; (e) Z^4 DAC − 500 (same data set as Fig. 1); (f) Z^5 DAC − 1000 (center frequency shifted −100 Hz).
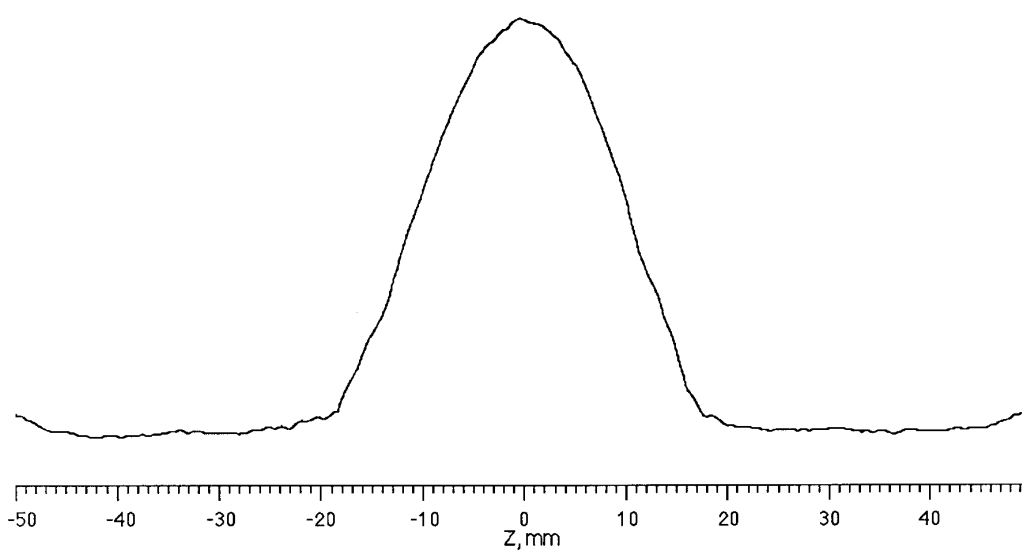
FIG. 3. 1D spatial image obtained by summing over all frequency components (i.e., coil sensitivity, or B_1 profile). Data for Z^4 coil—others are similar.
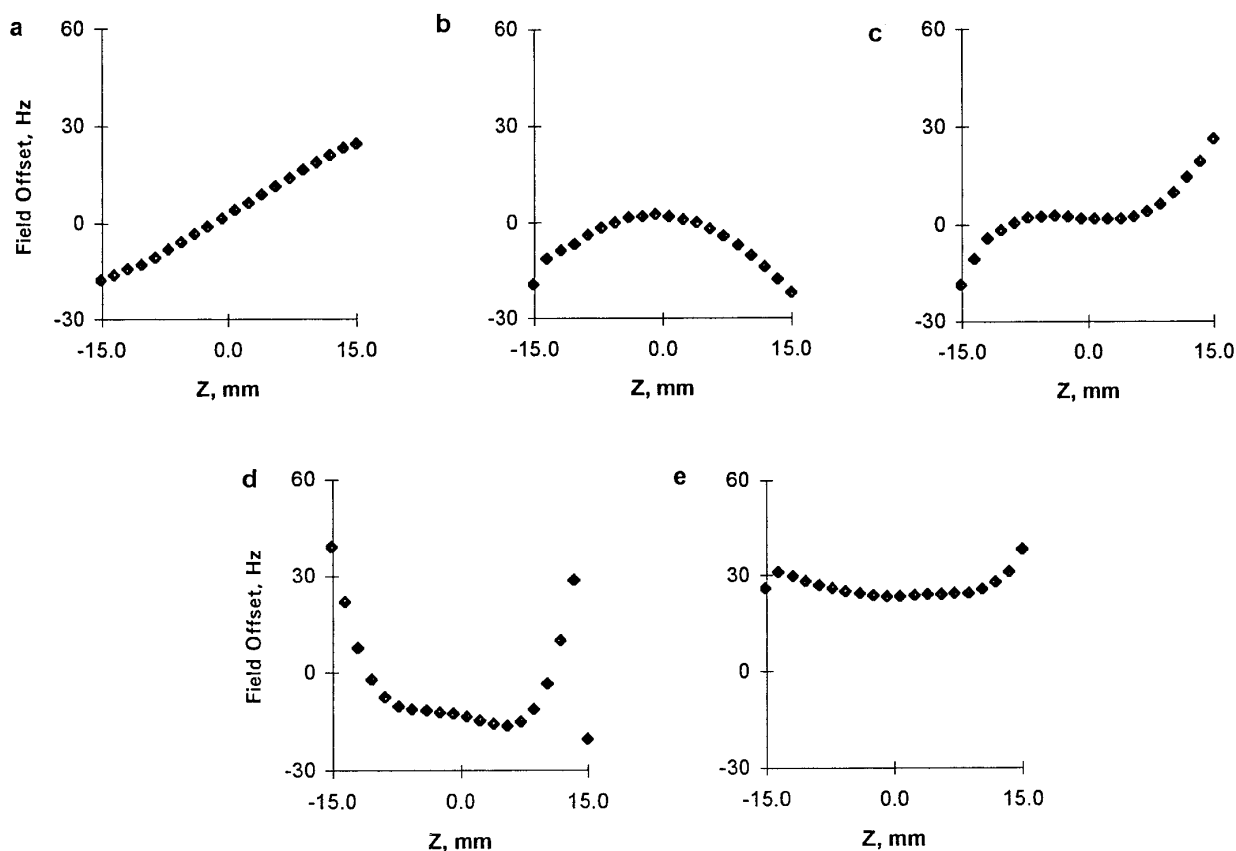
FIG. 4. Field plots for each of the shim coils, derived from the images in Fig. 2 by determining water peak frequency vs axial position and subtracting the reference field plot. (a) Z^1 fine DAC $-$ 400; (b) Z^2 fine DAC $-$ 800; (c) Z^3 fine DAC $-$ 700; (d) Z^4 DAC $-$ 500; (e) Z^5 DAC $-$ 1000.

the presence of even tiny off-resonance signals at the base of the water peak can produce enormous baseline artifacts. For comparison, the spectrometer's built-in simplex autoshim software was also used, starting from the same initial shim values and adjusting the same coils ($Z^1 - Z^5$). Au-

toshim took 8–10 min (about 100–120 trial acquisitions). The results are shown in Fig. 7.

DISCUSSION

PRSI Field Maps

The maps in Fig. 2 are easily interpreted, and clearly show the expected functional dependence of field on position for each coil. Even a single 1D map such as Fig. 2a can be instructive about field distortions. For example, it is evident

TABLE 1
Predicted DAC Values from LS Fitting of Perturbed Field to Shim Coil Maps

		Three coils perturbed			
Actual	−50	−50	−50		
Fit	−51.7	−14.4	−9.5		
SEE (±)[a]	2.8	5.3	7.4		
		Four coils perturbed			
Actual	−50	−50	−50	−50	
Fit	−41.1	−38.4	−68.3	−47.6	
SEE (±)	5.2	29.3	13.2	7.4	
		Five coils perturbed			
Actual	−50	−50	−50	−50	−50
Fit	−49.6	−55.3	−50.7	−38.0	−208.3
SEE (±)	8.2	38.0	21.5	8.5	71.1

[a] Standard error of least-squares (LS) parameter estimate.

TABLE 2
Correlation Coefficients between Shim Coil Maps over the Range +15 to −15 mm

	Z^1	Z^2	Z^3	Z^4	Z^5
Z^1	1.00				
Z^2	0.15	1.00			
Z^3	0.85	0.33	1.00		
Z^4	−0.39	−0.93	−0.53	1.00	
Z^5	0.99	0.23	0.88	−0.45	1.00
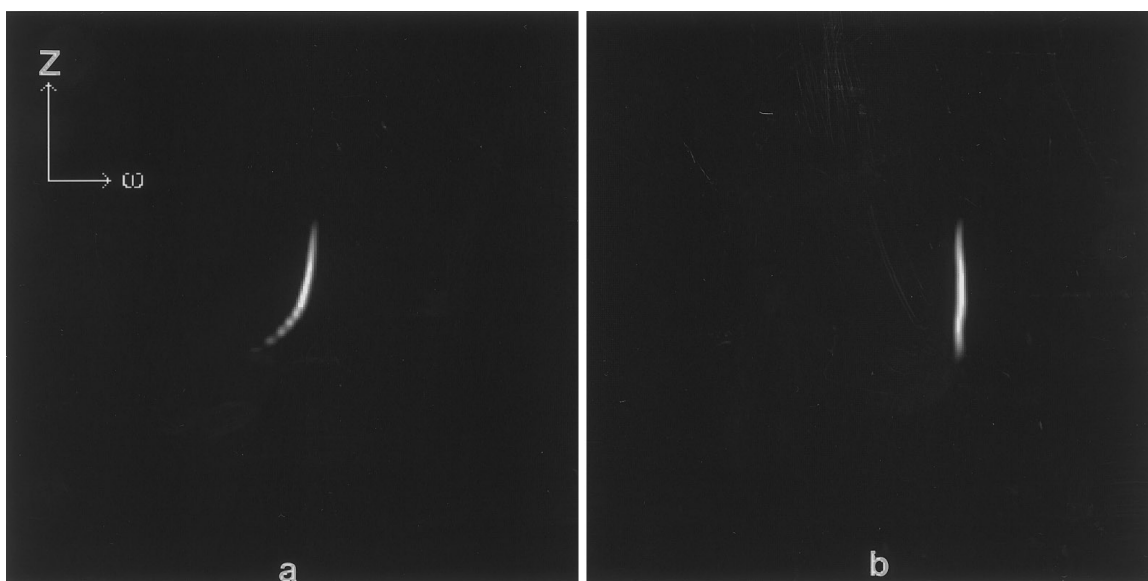
FIG. 5. Spectroscopic images of the sample of Fig. 2: (a) after moving the tube 10 mm; (b) after applying the correction determined from least-squares fitting to the individual coil fields.

that the reference state was not perfectly shimmed. There is a tail at the bottom of the probe which drifts toward lower frequency. Furthermore, the linewidth appears to vary somewhat across the sample, being larger at the ends. This is due in part to ray artifacts in the reconstruction from too few projections, but probably also in part to higher-order shims (such as Z^2X, for example) which were not exhaustively optimized prior to mapping.

PRSI is subject to a different sort of artifacts from the more familiar FSI (27). Of particular concern here are the ''ray'' artifacts which result from inadequate angular sampling. Relatively large numbers of projections (in the spectroscopic imaging context) were used, to minimize these artifacts. For the 1D + 1D SI case, this is not a particular drawback, since the data can still be acquired in a reasonable length of time. For generalization to 3D + 1D, for complete shimming of larger samples, one must contemplate methods for PRSI reconstruction from fewer angular projections (20, 23).

The conventional PR treatment, which simply uses a heavier high-frequency rolloff in filtering the projections in order to suppress ray artifacts, is not entirely appropriate here, since this also reduces the precision of the frequency maps. That is, one desires a much higher resolution along the frequency axis than along the spatial axis.

The B_1 field profile of the coil determines the sensitive volume, and the relative contribution of any off-frequency signal to the lineshape. From the profile in Fig. 1, it can be seen that the field drops to 50% of its peak value at ±11 mm from the center, and the signal within this volume is 82% of the total. Other points of possible interest are the 25% signal level (±14.5 mm, 93% of total) and the 10%

level (±17 mm, 96% of total signal). This particular coil is quite symmetric, and appears centered within the shim set to within 1 or 2 mm.

In principle, one would like to measure and shim the field over the entire region from which any signal can be observed. In practice, the precision of the field measurement decreases as the signal level decreases, for three reasons: (1) the line is broader due to high-order field terms, leading to some uncertainty in the frequency; (2) the back-projection algorithm introduces ray artifacts which may be mistaken for the signal from the sample, leading to errors in the field measurement; and (3) ordinary signal-to-noise and linewidth considerations make precise peak determination difficult. Thus there is a trade-off between the total acquisition time and accuracy (obtaining more projections both increases the signal-to-noise and reduces the ray artifact problem). There is also a trade-off between the shape of the central line and the intensity in any tails. For example, one can compensate the top and bottom of the tube using high-order axial terms, but this may result in some field ''wiggles'' causing broadening near the middle. The relative merits of different weighting functions depend, of course, on the intended application (8).

In practice, for the 64-projection sets used here, the field map could be reliably and automatically extracted only down to about 20–30% of the maximum signal intensity. Below this level, ray artifacts have amplitudes comparable to the true spectral peak, leading to erratic peak picking. Nevertheless, the map points above this threshold account for over 90% of the total observable signal, and appear to give useful results.

Shimming Results

As can be seen from Table 1, the shim corrections derived from the maps are not exact. This is not surprising in view
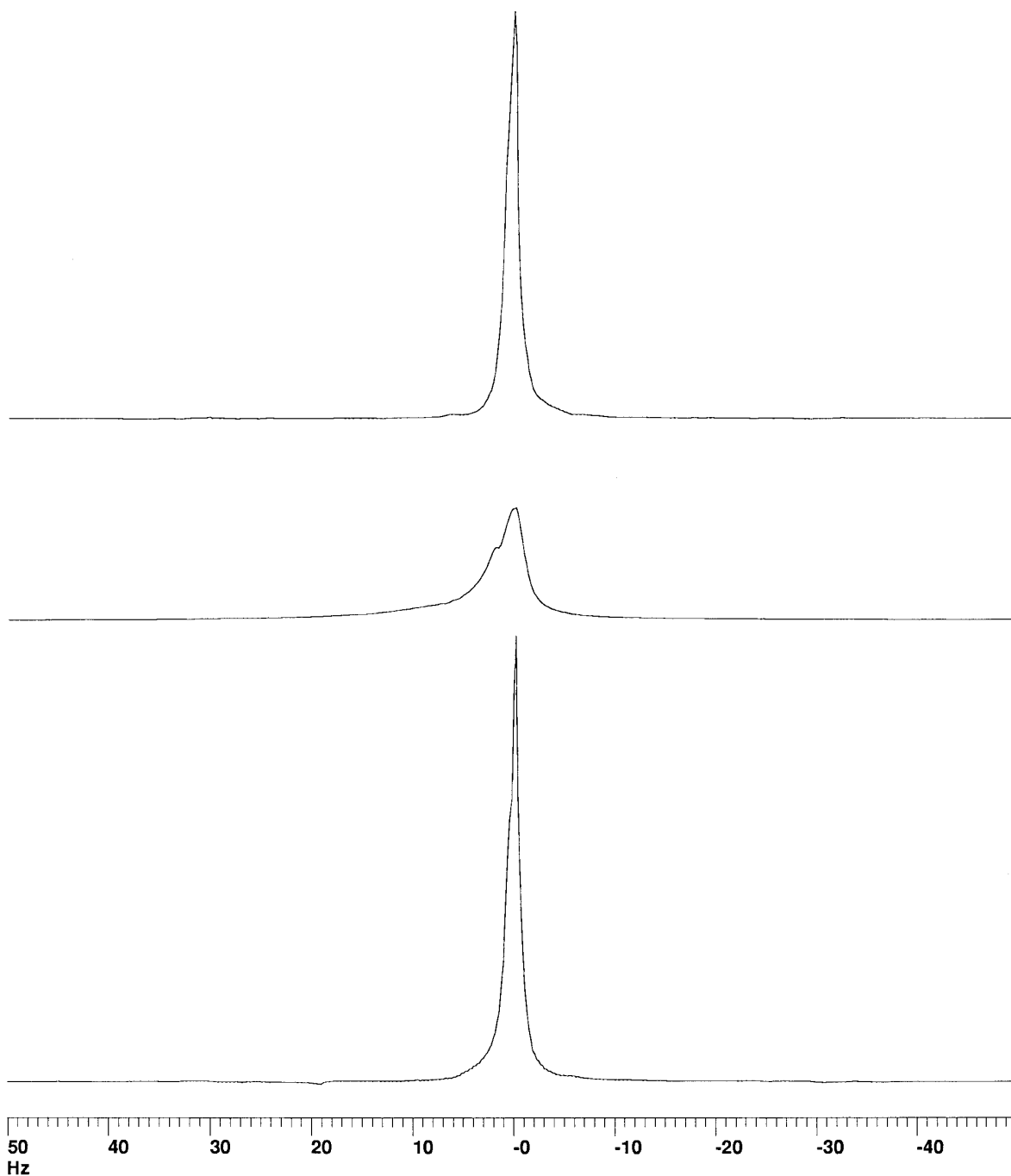
FIG. 6. Spectra corresponding to the images in Fig. 5, showing (bottom) initial spectrum; (middle) spectrum after moving sample tube 10 mm; and (top) spectrum after application of correction calculated from the field maps.

of some large correlations between individual shim coil effects, as shown in Table 2. Together with the inevitable uncertainty in the field values obtained from the maps (both test and reference maps contribute), this means that the estimated values may fall within a fairly wide range. In the language of matrix mathematics, the problem is ''ill conditioned.'' Although this might be disturbing, it simply means that this range of shim sets will give similar performance, a situation which is often observed in practice. It also means that the exact shim values chosen will depend on the criteria. For example, one may choose least-mean-square deviation (as used in this study), minimum peak–peak deviation, or some other criterion. Furthermore, one may choose to optimize the shims over any subset of the sensitive volume
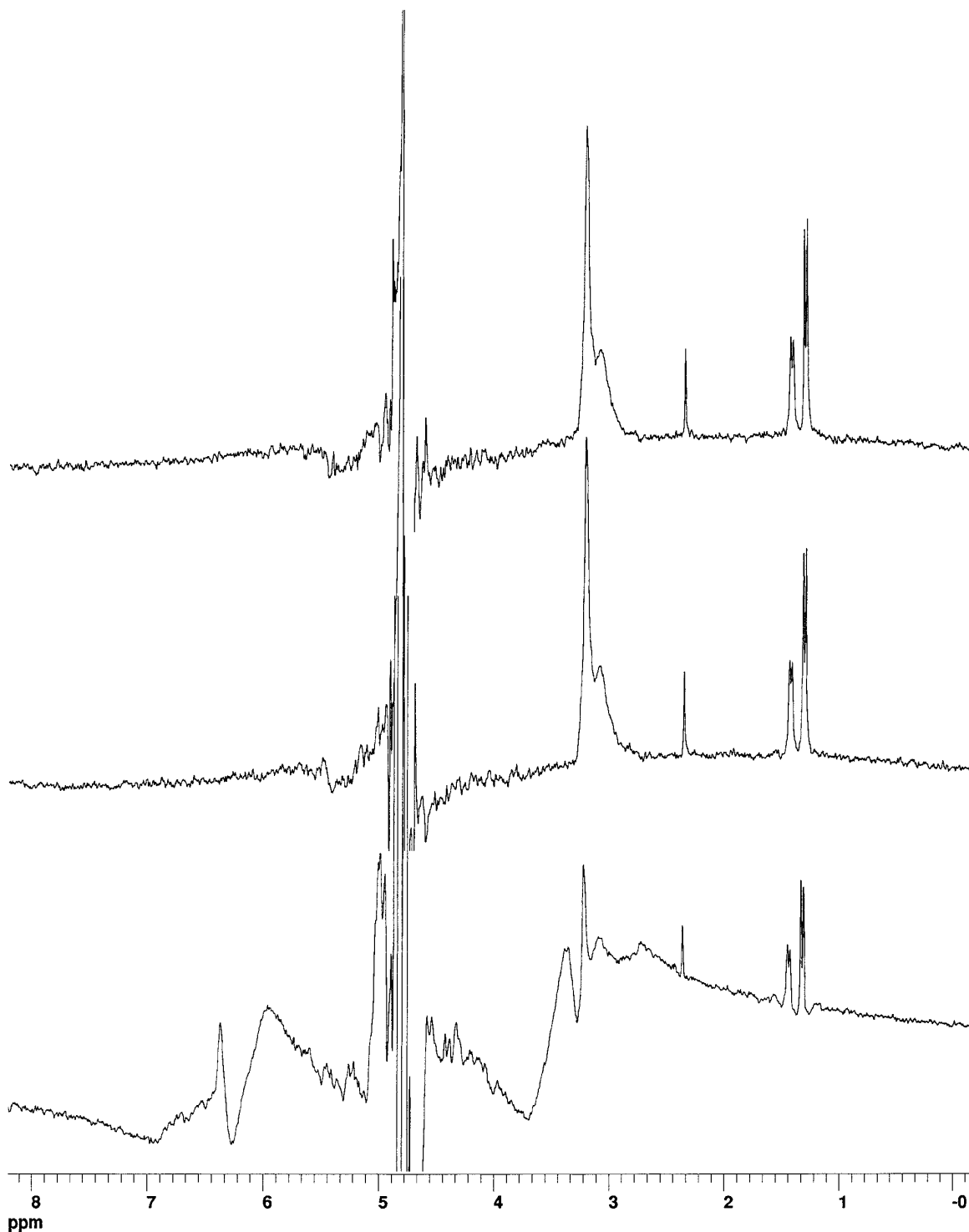
FIG. 7. Water suppression performance. (Bottom) Unshimmed sample (×0.5); (middle) shimmed from field maps (×1); and (top) shimmed by iterative simplex optimization (×1). 2 Hz line broadening. Peaks at 1.3 and 1.4 ppm are methyl of lactic acid and its dimer; at 2.3 ppm, an impurity; at 3–3.3 ppm, Pipes buffer.

where the frequency can be measured. In the latter case, the ill conditioning may be even more severe (*31*). Of course, this situation has nothing to do with PRSI, per se, but is

exactly the same as encountered in applying any other field mapping method.

In spite of the large standard error of the predicted DAC

values, the resulting spectra can be quite good. In particular, the water suppression performance of a single application of the correction algorithm (Fig. 7), based on a map obtained in 3 min, is essentially the same as that obtained by simplex autoshim requiring about 10 min. With a matched sensitivity-enhancement filter (2 Hz, Fig. 7), the methyl doublet of lactic acid ($J = 7$ Hz) is clearly resolved and the shimmed linewidths and shapes are very similar (FWHM = 4.0 Hz in each case). Although the linewidth reduction (from FWHM = 5.2 Hz before shimming) is small, the broad wandering baseline evident in the unshimmed spectrum is almost completely suppressed. This is a good demonstration of the danger of relying on single measures of field homogeneity, such as linewidth at half-height. Even an algorithm based on width at two levels, for example 50 and 10%, could be fooled into producing a poor baseline at the 0.55% level.

Comparison with Other Shimming Methods

In choosing a shimming technique, several considerations must be weighed: reliability, speed, availability of hardware and software, ease of use, and degree of automation. Some comparisons between the PRSI field mapping technique and other established techniques are thus appropriate.

The comparison here should be between mapping methods in general and single-response optimization methods. A further comparison between phase and frequency mapping is appropriate. Clearly, any method which yields a unique solution in one pass is superior to an iterative method which is subject to false optima. Frequency mapping has the further advantage that it does not suffer from phase wrapping or confusion due to multiple components. On these counts, PRSI and FSI are the imaging methods of choice.

The time required to generate a field map depends on the technique and the number of points (m) to be measured. For the 1D case with phase mapping, two acquisitions can each provide m samples of a projection, for each of which the phase difference can be determined. The time required is then simply $2T$, where T is the time required to do the data acquisition (typically the relaxation time of the sample). Frequency mapping requires a full spectrum at each point, thus requiring mT.

For the 1D case, and a typical spectrometer with five axial shims (Z^1–Z^5), m should be at least 6. Some overdetermination is desirable—in the results presented here, 64 projections were used, resulting in about 20 points over the sensitive volume. (Of course, because of the pointspread functions, adjacent points in PRSI or FSI are not entirely independent.) Since the number of acquisitions is small, however, the time penalty for using frequency mapping methods is not serious.

The time requirements for the 1D case are trivial—a complete field map using 64 projections is acquired in about 3 min, even with the slow software setup used here. The acquisition speed in our case is limited by the relatively slow software routine used to set up each projection (about 3 s per projection), although given the pace of computer speed improvement, this is clearly not an inherent limit.

Time becomes a much more important consideration when 3D shimming is required—64^3 projections would be prohibitive in most cases. Various options for reducing the required number of projections are being investigated in connection with development of the 3D + 1D PRSI technique. Preliminary results (35) indicate that usable 3D + 1D maps can be obtained with only 12^3 projections, and it may be possible to reduce this to 8^3, while still retaining the back-projection-reconstruction method. With 8^3 projections acquired at 2 s per projection, a complete 3D + 1D map could be obtained in about 20 min, including processing. This is a reasonable price to pay in spectrometer time for difficult shimming situations. A similar number of acquisitions would also be required for a Fourier spectroscopic imaging experiment. For comparison, typical simplex autoshim runs, using all 18 shim channels together or in groups, require a similar amount of time, but with little likelihood of convergence unless the correct starting point is chosen. Alternate reconstruction methods, such as iterative reconstruction ($20, 23$) or interpolation and Fourier transform (36), might make it possible to use even fewer projections to obtain usable maps.

Older spectrometers, without pulsed field gradients, are inherently incapable of executing any of the standard PFG imaging experiments. Thus only methods with static gradients, such as PRSI, are feasible. PRSI is in principle even compatible with a CW instrument, where it could be done by hand, given enough patience. Furthermore, PRSI is applicable to samples with short T_2's, where echo-based imaging methods may fail (although extremely short T_2's may make field mapping for shimming less important).

Another possible alternative for older instruments is the phase mapping method based on ''constant-time imaging'' (15), using static phase-encode gradients. In spite of being a phase mapping technique, this requires essentially the same time mT as a full Fourier SI experiment, since only one pair of samples is acquired for each gradient setting and acquisition. Thus it is at a disadvantage with respect to any frequency mapping experiment, which requires the same time but produces a less ambiguous result.

A barrier to use of this (or any) mapping technique is the absence of integrated software for spectrometer control and data analysis. In principle, of course, this can be overcome. A software package should permit automatic acquisition of the data, compute the maps, fit to a set of reference data, and produce a set of shim DAC values for operator approval. Advanced features might include graphical specification of the volume to be shimmed, or storage of a measured field map for deconvolution of spectral lines in subsequently acquired data. Although not fully integrated, the software used in this report is all available commercially, in the public

domain, or in the case of the instrument automation scripts, upon request from the author,[1] for those who wish to implement the procedure for themselves.

CONCLUSION

PRSI permits *in situ* field mapping on a conventional NMR spectrometer, equipped only with shim coils, where other field mapping techniques are impossible. Even 1D maps can be instructive about sample, probe, or magnet inhomogeneities. The availability of field maps offers the possibility of accurately and automatically shimming an NMR spectrometer, more reliably than iterative search techniques commonly used for the purpose today. Successful axial shimming using 1D + 1D PRSI has been demonstrated. No fundamental barriers exist to full mapping and shimming using 3D + 1D PRSI.

ACKNOWLEDGMENTS

REFERENCES

1. W. Conover, *in* ''Topics in Carbon 13 Magnetic Resonance Spectroscopy'' (G. Levy, Ed.), Vol. 4, Chap. 2, p. 37, Wiley, New York (1984).

2. G. N. Chmurny and D. I. Hoult, *Concepts Magn. Reson.* **2,** 131 (1990).

3. V. W. Miner and W. W. Conover, *in* ''Encyclopedia of Nuclear Magnetic Resonance'' (D. M. Grant and R. K. Harris, Eds.), Vol. 7, p. 4340, Wiley, Chichester (1996).

4. J. A. Nelder and R. Mead, *Comput. J.* **7,** 308 (1965).

5. F. Romeo and D. I. Hoult, *Magn. Reson. Med.* **1,** 44 (1984).

6. K. Sekihara, S. Matsui, and H. Kohno, *J. Phys. E* **18,** 224 (1985).

7. I. S. Mackenzie, E. M. Robinson, A. N. Wells, and B. Wood, *Magn. Reson. Med.* **5,** 262 (1987).

8. M. G. Prammer, J. C. Haselgrove, M. Shinnar, and J. S. Leigh, *J. Magn. Reson.* **77,** 40 (1988).

9. J. Tropp, K. A. Derby, C. Hawryszko, S. Sugiura, and H. Yamagata, *J. Magn. Reson.* **85,** 244 (1989).

10. P. Webb and A. Macovski, *Magn. Reson. Med.* **20,** 113 (1991).

11. E. Schneider and G. Glover, *Magn. Reson. Med.* **18,** 335 (1991).

12. R. Gruetter and C. Boesch, *J. Magn. Reson.* **96,** 323 (1992).

13. P. C. M. van Zijl, S. Sukumar, M. O'Neil Johnson, P. Webb, and R. E. Hurd, *J. Magn. Reson. A* **111,** 203 (1994).

14. J. Hu, T. Javaid, F. Arias-Mendoza, Z. Liu, R. McNamara, and T. R. Brown, *J. Magn. Reson. B* **108,** 213 (1995).

15. S. Sukumar, M. O'Neil-Johnson, and J. A. B. Lohman, 37th Experimental NMR Conference, Abstract WP 206 (1996).

16. C. Pedersen, N. Bansal, and R. L. Nunnaly, *Radiology* **173P,** 380 (1989).

17. A. A. Maudsley, A. Oppelt, and A. Ganssen, *Siemens Forsch. Entwickl. Ber.* **8,** 326 (1979).

18. P. C. Lauterbur, D. N. Levin, and R. B. Marr, *J. Magn. Reson.* **59,** 536 (1984).

19. M. L. Bernardo, Jr., P. C. Lauterbur, and K. L. Hedges, *J. Magn. Reson.* **61,** 168 (1985).

20. A. E. Stillman, D. N. Levin, D. B. Yang, R. B. Marr, and P. C. Lauterbur, *J. Magn. Reson.* **69,** 168 (1986).

21. M. M. Maltempo, *J. Magn. Reson.* **69,** 156 (1986).

22. M. M. Maltempo, S. S. Eaton, and G. R. Eaton, *J. Magn. Reson.* **72,** 449 (1987).

23. M. M. Maltempo, S. S. Eaton, and G. R. Eaton, *J. Magn. Reson.* **77,** 75 (1988).

24. M. M. Maltempo, S. S. Eaton, and G. R. Eaton, *in* ''EPR Imaging and in Vivo EPR'' (G. R. Eaton *et al.,* Eds.), Chap. 13, CRC Press, Boca Raton, FL (1991).

25. G. R. Eaton and S. S. Eaton, *Concepts Magn. Reson.* **7,** 49 (1995).

26. P. Kuppusamy, M., Chzhan, A. Samouilov, P. Wang, and J. L. Zweier, *J. Magn. Reson. B* **107,** 116 (1995).

27. R. K. Woods, W. B. Hyslop, R. B. Marr, and P. C. Lauterbur, *in* ''EPR Imaging and in Vivo EPR'' (G. R. Eaton *et al.,* Eds.), Chap. 10, CRC Press, Boca Raton, FL (1991).

28. R. K. Woods, W. B. Hyslop, and H. M. Swartz, *Phys. Med.* **5,** 121 (1989).

29. W. B. Hyslop, R. K. Woods, and P. C. Lauterbur, *IEEE Trans. Med. Imaging* **14**(2), 374 (1995).

30. D. I. Hoult, C-N. Chen, H. Eden, and M. Eden, *J. Magn. Reson.* **51,** 110 (1983).

31. D. I. Hoult, *J. Magn. Reson.* **73,** 174 (1987).

32. V. Sklenar and A. Bax, *J. Magn. Reson.* **74,** 469 (1987).

33. C. S. Potter and P. J. Moran, Viewit: A software system for multidimensional biomedical image processing, analysis, and visualization,'' *SPIE Conference on Biomedical Image Processing and Three-Dimensional Microscopy, Vol. 1660,* pp. 767–773 (1992). Additional information available at URL http://kepler.ncsa.uiuc.edu/viewit.html.

34. H. Barjat, P. B. Chilvers, B. K. Fetler, T. J. Horne, and G. A. Morris, *J. Magn. Reson.* **125,** 197 (1997).

35. C. D. Gregory, C. S. Potter, H. D. Morris, and P. C. Lauterbur, 38th Experimental NMR Conference, Abstract P143 (1997).

36. H. Stark, J. W. Woods, I. Paul, and R. Hingorani, *IEEE Trans. Acoust. Speech Signal Process.* **29,** 237 (1981).

---

[1] Scripts and macros for acquiring and processing 2D (and 4D) PRSI data are available on the World Wide Web and may be downloaded from the URL http://bmrl.med.uiuc.edu:8080/~cgregory/prsi/index.html.